Geomechanics and Engineering, *Vol. 39, No. 4 (2024) 357-368*
https://doi.org/10.12989/gae.2024.39.4.357

Experimental research on the tensile properties of coal rocks in deep old goafs

Ning Jiang*[1,2], Quanbao Su**[1], Xia Jiang[4], Zhiyou Gao[1,3], Qingbiao Guo[5], Shijie Song[6], Tao Lyu[1,3] and Ke Lyu[7]

[1]*College of Energy and Mining Engineering, Shandong University of Science and Technology, Qingdao 266590, China*
[2]*State Key Laboratory of Mine Disaster Prevention and Control, Shandong University of Science and Technology, Qingdao 266590, China*
[3]*Shandong Geology and Mineral Resources Engineering Group Co., Ltd., Jinan 250013, China*
[4]*Yuloka (Shandong) Mining Technology Co., Ltd.,Taian 271000, China*
[5]*School of Spatial Informatics and geomatics Engineering, Anhui University of Sciences and Technology, Huainan 232001, China*
[6]*College of Geology& Environment, Xi'an University of Science and Technology, Xi'an 710054, China*
[7]*School of Mines, China University of Mining and Technology, Xuzhou, Jiangsu, 221116, China*

(*Received March 26, 2024, Revised October 16, 2024, Accepted November 11, 2024*)

Abstract. The pressurized water conditions of goafs weaken the support of remaining coal and rocks, which causes instability, failure, and sudden ground collapse. The impact of pressure-bearing water and CO_2 on the tensile properties of residual coal pillars was explored in old goafs. Coal was analyzed using a pressure-water soaking device, electronic scanning microscope, and 3D full-field strain measurement system. Besides, Brazilian splitting tests were performed. The failure characteristics and energy evolution law of the macro-microscopic structure of coal specimens were analyzed under different soaking conditions—desiccation (DC), CO_2 soaking (CS), water-CO_2 soaking (WCS), and water soaking (WS). The peak stress of coal specimens and time to reach the peak decreased with varying soaking environments. Stress concentration initially occurred at the water end under the WCS condition, indicating that coal specimens deteriorated more under the pressure-bearing WCS condition compared with the CS condition. Fractures of coal specimens exhibited the highest development under the WS condition. Besides, dissolution was observed at the fractures of coal specimens, with severe failure to their internal microstructures. In conclusion, the instability failure of residual coal pillars is significant in studying the old goafs.

Keywords: Brazilian splitting test; mesoscopic analysis; soaking condition; tensile strength of coal rocks; water-CO_2 action

1. Introduction

Despite variations in the energy structure, China's coal resources account for over 50% of total energy, which is crucial for infrastructure construction and the economy (Zhang *et al.* 2023, Ji *et al.* 2023). Coal persists as the main energy source for an extended period (Gong *et al.* 2021) in the production and consumption structure of primary energy in China. The energy supply-side structure has undergone reform, which eliminates outdated production capacity in the energy industry. Some mines are out of service life or unsafe for production. Therefore, they are facing closure or abandonment, which increases the number of abandoned mines. There will be 15,000 closed/abandoned mines in China by 2030. The direct closure or abandonment of such mines can cause significant resource wastage and the loss of state-owned assets. Besides, it may induce safety and environmental concerns. (Morris *et al.* 2005, Li *et al.* 2023).

Previously, different types of protective coal pillars are implemented around the quarry (sectional coal pillars, strip coal pillars, and room-and-pillar coal pillars) (Li *et al.* 2022, Lbishi *et al.* 2022). for safe, efficient, and environmentally friendly mining. The closure of the mining lot and cessation of dredging increases the underground water level. Besides, the pores and fractures of coal-rock mass exhibit strong anisotropy (Song *et al.* 2023, Yin *et al.* 2019, Xie *et al.* 2023, Xia *et al.* 2020). Mining voids are backfilled, and the residual coal pillars are subjected to pressure-bearing water and CO_2. Therefore, the supporting performance of coal pillars deteriorates, which causes instability failure. Then, coal-rock mass stabilizes and sudden waterlogging may occur in abandoned areas (Hu *et al.* 2010, Chen *et al.* 2023, Li *et al.* 2023). Therefore, the pressure-bearing water-immersed environment is crucial for studying the long-term stability and instability failure of residual coal pillars in the old goafs.

Researchers have studied the deterioration of the mechanical properties of coal rocks (Shi *et al.* 2019, Komurlu *et al.* 2016, Wang *et al.* 2022, Zhang *et al.* 2023, Qu and Tao 2019, Heidari *et al.* 2011). A discrete element method (DEM) called particle flow code (PFC2D) is used to construct a model for the Brazilian disc splitting test (Yang and Huang 2015). Based on the experimental results of an intact Brazilian disc of rock-like material, a set of micro-parameters in PFC2D that reflecting the macro-mechanical behavior of rock-like materials are obtained.

*Corresponding author, Ph.D.
E-mail: jiangning@sdust.edu.cn
**Mr.S.
E-mail: suquanbao@163.com

ISSN: 2005-307X (Print), 2092-6219 (Online)

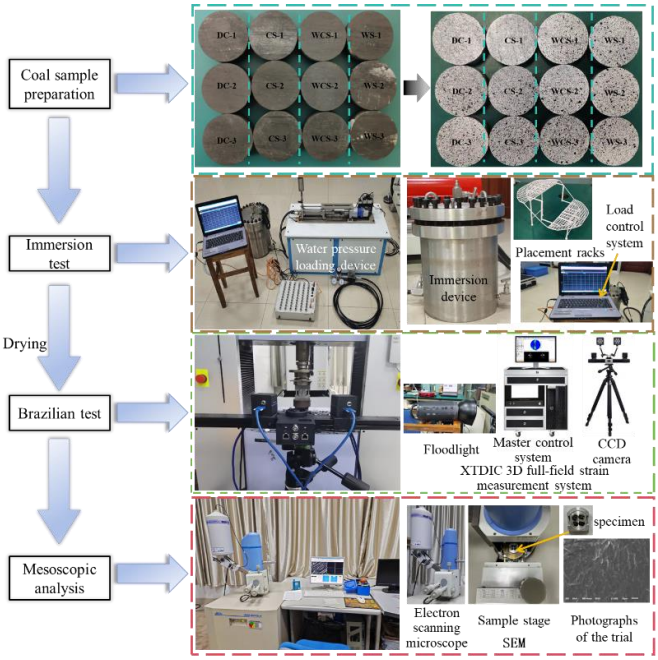

Fig. 1 Experimental flow

Guo *et al.* (2024) was found that the entire loading process in the Brazilian splitting test mainly consists of compaction, elasticity, and post-peak decline stages, without a distinct yielding stage.

Based on the numerical simulation, the concentrated load of the perforated Brazilian disc is simulated by Bai *et al.* (2016). Chen *et al.* (2022) combined with a uniaxial compression test and two-dimensional particle flow software (PFC2D), the mechanical properties and failure modes were explored. Zhao *et al.* (2021) studied the tensile failure characteristics of dry and water-saturated coals under different impact loading conditions using a Split Hopkinson pressure bar. Bilgen *et al.* (2019) proposed an improved phase-field method for handling fracture issues, which is capable of locating the position of cracks, determining the stress distribution within (cracking) specimens, and quantifying the tensile resistance of materials.

Vásárhelyi and Ván (2006) studied the impact of water on the tensile strength of rocks and proposed a computational method to quantify the extent of strength attenuation in waterstone. Zhao *et al.* (2018) conducted uniaxial compression deformation tests, Brazilian splitting tests, and cornea pressure shear tests on rocks from the Dajishan tungsten mine. Essential mechanical parameters, including the internal friction angles of both the ore rock and the surrounding rock, are determined through these tests. Additionally, an in-depth study and analysis of the damage characteristics of the rocks are performed under different experimental conditions. Miehe *et al.* (2010) introduced a fracture model to present the evolution of coal rocks under the influence of local variables based on solid fractures.

These studies are crucial for comprehending the tensile properties and deterioration mechanism of coal rocks under pressure-bearing water and CO_2. However, residual coal pillars in old goafs, subjected to pressure-bearing water and CO_2 all year round, tend to lose stability. Therefore, the work analyzed the tensile properties and deformation failure characteristics of coal specimens under pressure-bearing water and CO_2 through Brazilian splitting tests, XRD, XRF, and mesoscopic analysis. The deterioration mechanism of coal rocks' tensile strength under pressure-bearing water and CO_2 was significant for understanding the stability of residual coal pillars in old goafs.

2. Test system and methods

2.1 Test plan and materials

Coal specimens were collected from a specific location within a mine in Shandong to minimize the impact of discrete specimens on test results. The tensile properties of coal specimens were studied under pressure-bearing water and CO_2. Twelve coal specimens were prepared in the test, and each group contained 3 coal specimens, making a total of 4 groups (Fig. 1). The diameter and thickness of coal specimens were 50 mm and thickness was 25 mm, respectively. Moreover, coal specimens had a non-parallelism of the smooth end face less than 0.05 mm, and the deviation of upper and lower end faces was less than 0.02 mm. Guo *et al.* (2021). Test errors caused by stress concentration were avoided due to irregular specimens (Lyu *et al.* 2024).

Coal specimens were placed into an independently developed coal-rock pressure-water soaking experimental device in the soaking test (Yin *et al.* 2022). Three kinds of soaking conditions were realized through the placement frame. The uppermost corresponded to CO_2 soaking (CS group); the second layer corresponded to water-CO_2 soaking (WCS group); the bottom layer corresponded to

Table 1 Brazilian splitting test results for coal specimens

Group	Value taking	*P*(kN)	σ_t (MPa)	Deterioration(%)
DC	Minimum-Maximum	2.87-3.2	1.46-1.63	0
	Mean value	3.08	1.57	
CS	Minimum-Maximum	2.47-2.81	1.26-1.43	14
	Mean value	2.64	1.35	
WCS	Minimum-Maximum	1.86-2.14	0.95-1.09	36
	Mean value	1.96	1	
WS	Minimum-Maximum	0.92-1.47	0.47-0.75	59
	Mean value	1.26	0.64	

CO_2 soaking (WS group). The barrel was initially filled with an appropriate amount of distilled water. Subsequently, the soaking device was supplied with water via the water-pressure loading device until the upper drain experienced water overflow. Then, the switches of the soaking device were closed, and the air intake switch was turned on to introduce CO_2. The pressure was set to 5 MPa, and water was discharged from the bottom drain. The water level was adjusted to 120 mm and the soaking duration was set to 15 d. Soaked specimens were removed for drying in preparation for the Brazilian splitting test after soaking. The fragments at the fracture of coal specimens were scanned by Apreo high-resolution scanning electron microscopy (SEM). The mesoscopic analysis of coal specimens' tensile properties was carried out to explore the influence of soaking conditions on them.

2.2 Testing equipment

The main control system and monitoring system of the Brazilian splitting test included the loading system, XTDIC 3D full-field strain measurement system, and SEM. The laboratory, loading system, and strain measurement system were synchronized to ensure the same time parameters for data processing and analysis. The loading system was a Shimadzu AG-X250 electronic universal testing machine driven by AC motor servo. The loading method adopted a double screw assembly. Equipment was stable with high accuracy. Conventional compression, stretching, and other mechanical experiments were realized at a maximum load of 250 KN. Control loading was used during the test, and the loading direction was parallel to the bedding plane of coal specimens at 0.05 kN/s

The XTDIC 3D full-field strain measurement system consisted of a CCD camera, image capture card, monitor, and computer. The speckle field was made on the surface of coal specimens by artificial spraying. The CCD camera stored acquired digital images in the computer when it shot the surface of specimens sprayed with artificial speckles.

The speckle map was analyzed to obtain the deformation and failure law of coal rocks after the test. SEM was an Apreo high-resolution scanning electron microscope. The meso-mechanism of the influence of different soaking conditions on the tensile properties of coal specimens was revealed by scanning specimens' fractures using SEM.

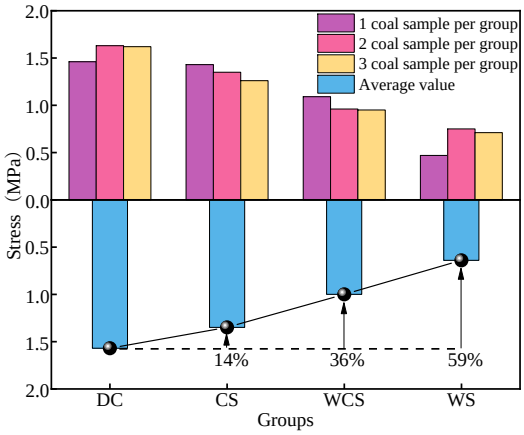

Fig. 2 Relationship between the tensile strength of coal specimens and soaking conditions

3. Test results and analysis

3.1 Brazilian splitting test analysis

Tensile strength (σ_t) (Akin and Likos 2017) and the deterioration degree of average tensile properties during the Brazilian splitting was calculated from the applied compressive force with failure (P) and the diameter (D) and thickness(t) of the specimen according to Eq. (1)

$$\sigma_t = \frac{2P}{\pi Dt} \tag{1}$$

The tensile strength of coal specimens in the WS group is the weakest at 0.64 MPa (Fig. 2). In contrast, strength in the DC group is the greatest at 1.57 MPa. The average deterioration of coal specimens' tensile strength in CS, WCS, and WS groups is reduced by 14, 36, and 59%, respectively, compared with that in the DC group. The CS condition affects least the deterioration of coal specimens' tensile strength. The WS condition has the greatest impact followed by the WCS condition. The deterioration of coal specimens' tensile strength is primarily influenced by pressure-bearing water and CO_2 under the WS condition.

Fig. 3 shows the tensile strength of coal specimens. The stress-time curve of coal specimens under the DC condition follows the same law under soaking conditions. They go through the intensified fracture, unstable fracture development, and post-fracture stages. Significant drops or fluctuations indicate brittle coal specimens. Brittleness index $\boldsymbol{\delta}$ of coal rocks can be defined as the ratio of peak stress to time according to research (Yagiz 2008).

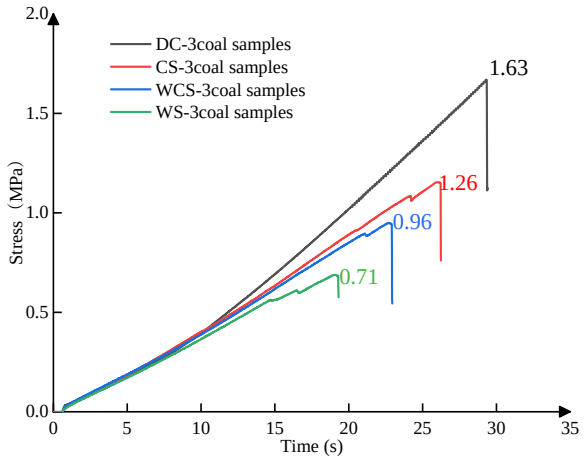

Fig. 3 Stress-time curves of coal specimens

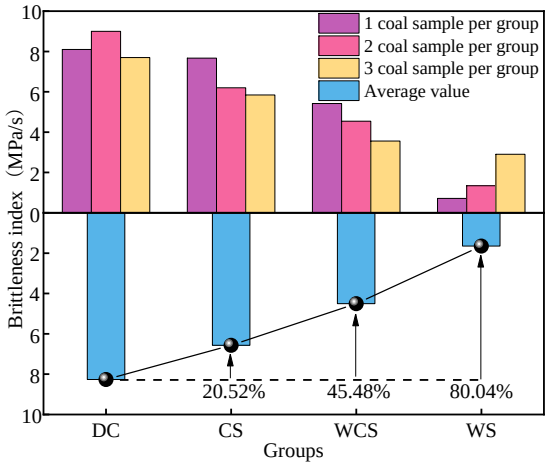

Fig. 4 Brittleness index of coal specimens

Fig. 4 illustrates the variation trend in $\boldsymbol{\delta}$ of four groups of coal specimens. Average $\boldsymbol{\delta}$ of coal specimens in the DC group is maximum (8.27 MPa/s); average $\boldsymbol{\delta}$ of coal specimens in the WS group was minimum (1.65 MPa/s). Average $\boldsymbol{\delta}$ of coal specimens in CS, WCS, and WS groups are reduced by 20.52, 45.48, and 80.04% compared with that in the DC group. The brittleness index decreases after soaking. The water-soaking condition reduces the brittleness index of coal specimens most, followed by the WCS condition. CS affects the brittleness index of coal specimens the least.

3.2 Deformation and failure characteristics

The macroscopic fracture propagation of coal specimens' carrying capacity are described under the evolution of the localized deformation zone as well as pressure-bearing water and CO_2. Coal specimens of DC-1, CS-1, WCS-1, and WS-1 are selected after the test. The evolutionary characters of the localized deformation zone are analyzed through displacement evolution.

First, the localized deformation zone of the main strain cloud map is divided before the ultimate failure of coal specimens. Then, the displacement dislocation method on

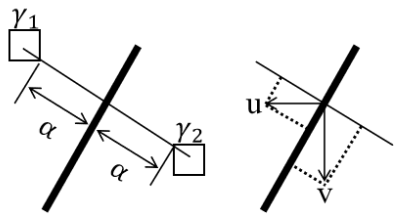

Fig. 5 Displacement on both sides of the localized deformation zone

both sides of the localized deformation zone (Liu *et al.* 2020) (Fig. 5) is used to calculate the displacement dislocation of four groups of coal specimens. α (α = 2 mm) is the distance between the two sides of the localized deformation zone marking line; points γ_1 and γ_2 are the corresponding areas of the center point; u is the horizontal displacement of selected pixels; v is the vertical displacement of selected pixels. The displacement dislocation in the counterclockwise direction is positive.

The evolution law of the maximum main strain field and displacement dislocation at the beginning of the evolution is analyzed. Four characteristic stages on the stress-time curve are selected. They are fracture compaction stage (points A and B), elastic deformation stage (points B and C), unsteady fracture development stage (points C and D), and post-fracture stage (after point D). Original macroscopic fractures are marked with blue lines, and the newborn ones are marked with red lines

Coal specimens become intensified at the fracture compaction stage (points A and B) (Fig. 6). The surface deformation is subtle, and original internal pores and fractures are compacted and filled. DC-1, CS-1, WCS-1, and WS-1 specimens exhibit varying stress concentration. WCS-1 and WS-1 coal specimens show obvious equipotential line concentration at the soaked end of the strain cloud map. Besides, the displacement dislocation of the WS-1 specimen is significant accompanied by a few macroscopic fractures. DC-1 and CS-1 coal specimens produce a minor alteration in the displacement dislocation. Therefore, the deterioration of coal specimens under the water-soaking condition is less significant than that under the CS condition.

The strain equipotential line on the surface of coal specimens draws close to the original fractures in the elastic deformation stage (points B and C). It aggregates at fractures with the increased stress. A localized deformation zone is formed at fractures after the internal fractures of coal specimens are completely compacted. Coal specimens of CS-1, WCS-1, and WS-1 exhibit denser-strain equipotential lines and wider localized deformation zones compared with those of DE-1. Localized deformation zones H, I, and J in the case of FW-1 exhibit an initial displacement dislocation, which increases incrementally. The strain equipotential line of coal specimens draws close to the localized deformation zone. New fractures appear in coal specimens in pressure-bearing water and CO_2, indicating the development and expansion of macroscopic fractures.

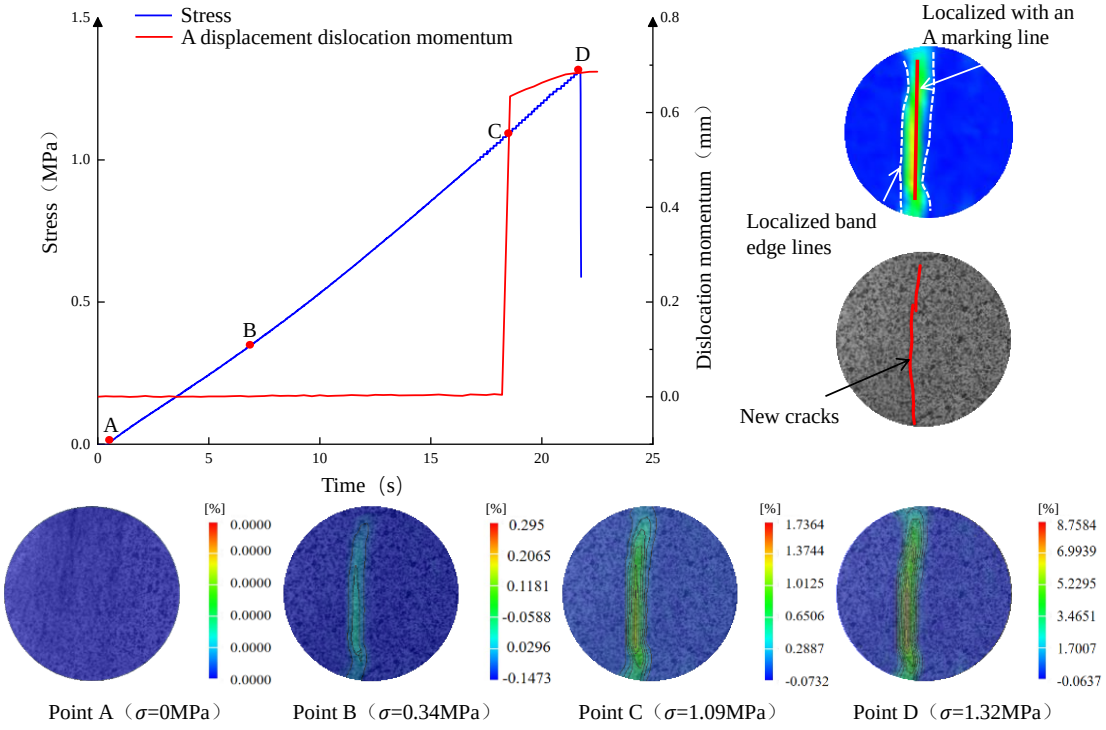

(a) DC-1

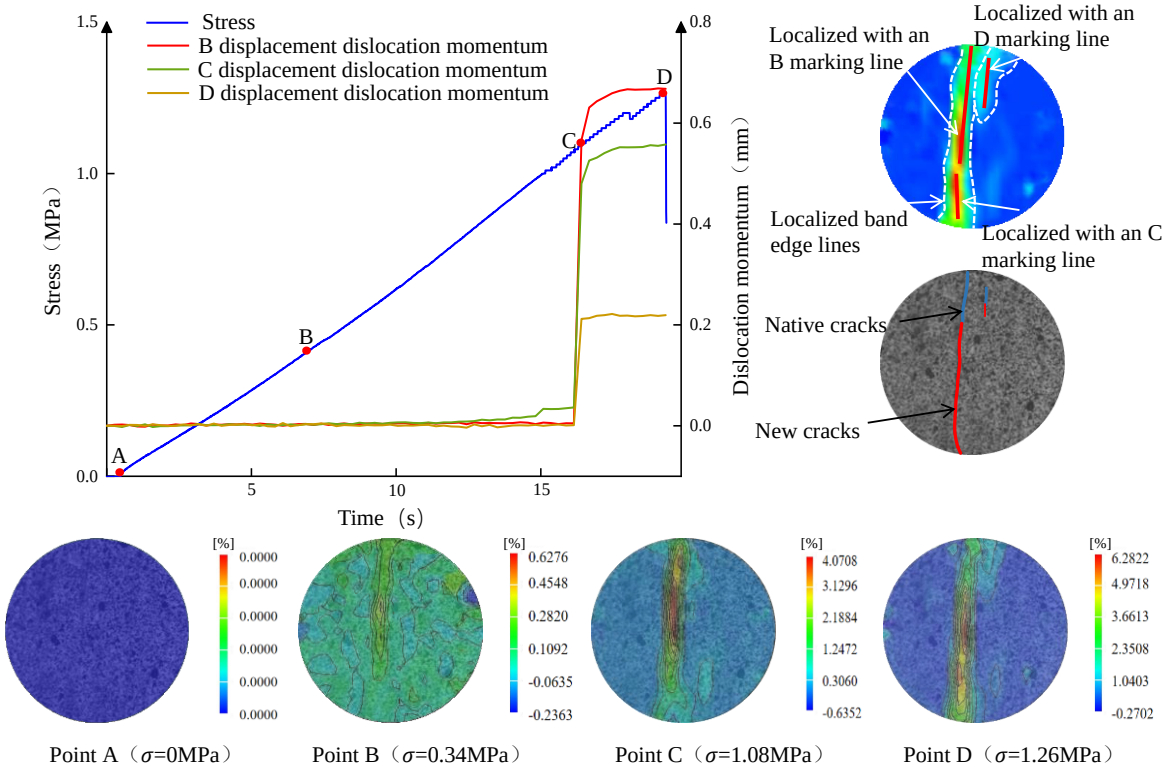

(b) CS-1

Fig. 6 Evolution of the maximum strain field of coal specimens

Coal specimens lose the carrying capacity when the stress is loaded from points C to D. The localized deformation zone further expands and generates a macroscopic main failure surface at an angle to the axial direction. The strain equipotential line converges towards the localized deformation zone of the main macroscopic tensile fractures. The main fractures produced by the DC-1 coal specimen are mainly caused by tensile deformation failure with a maximum displacement dislocation of 0.64 mm.

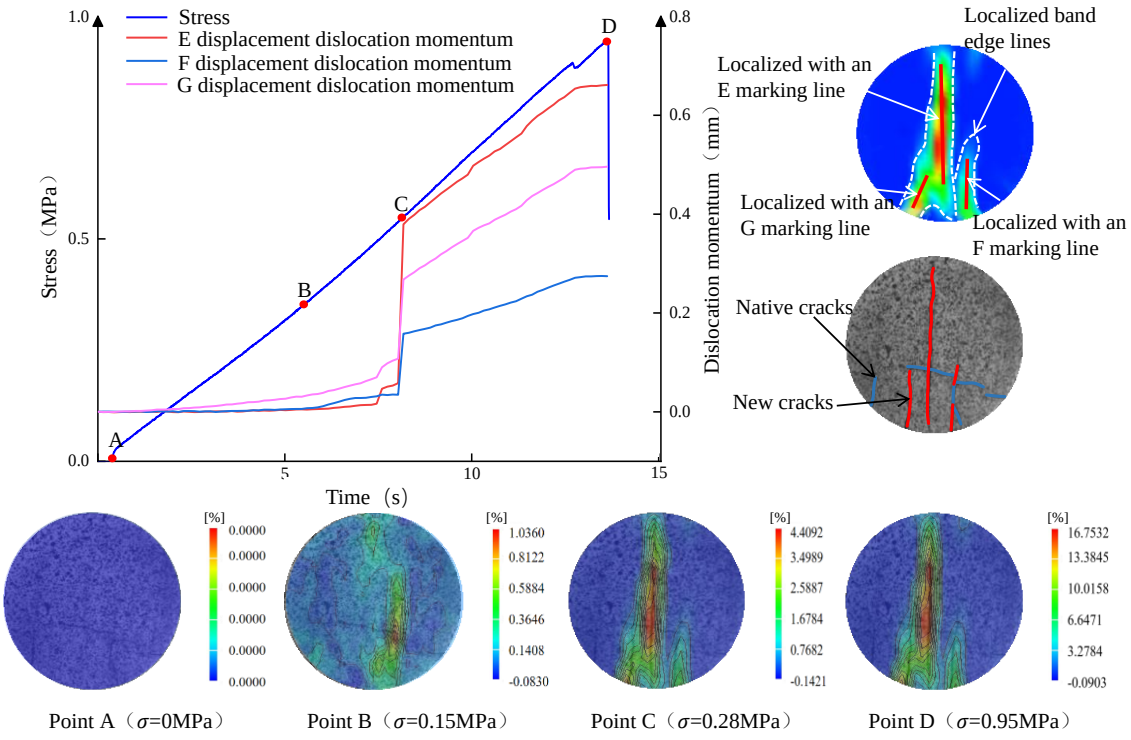

(c) WCS-1

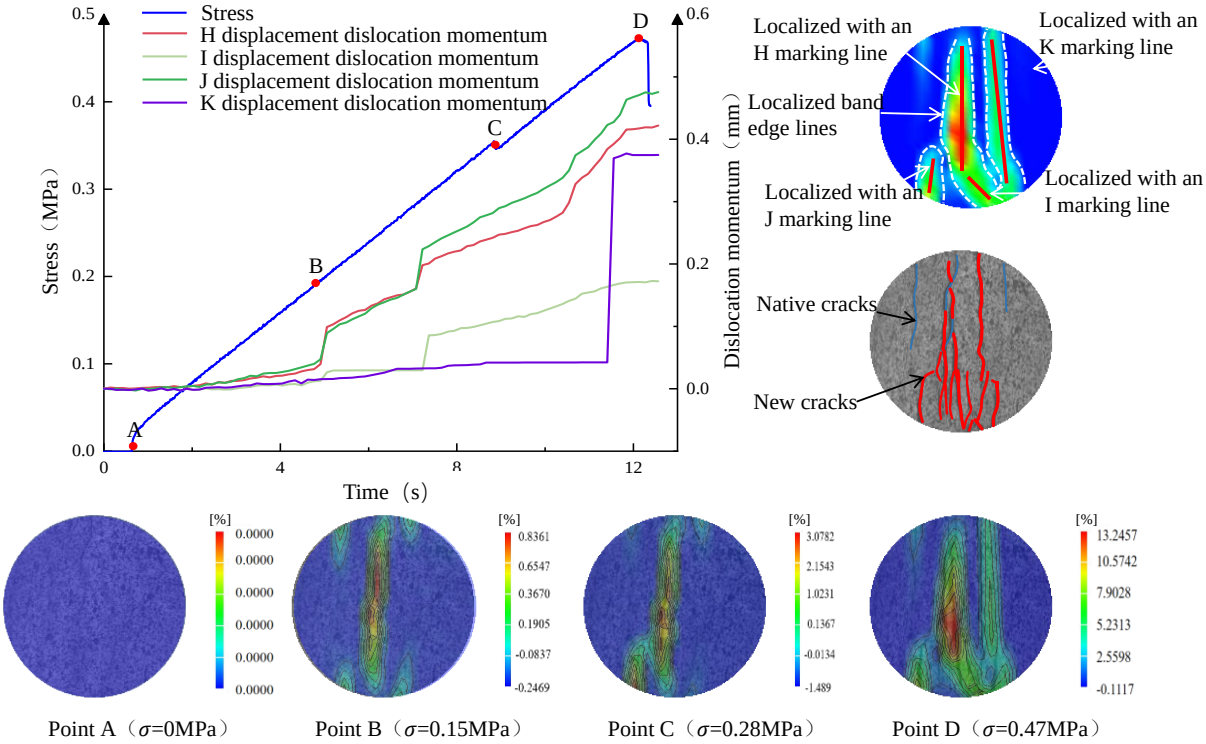

(d) WS-1

Fig. 6 Continued-

CS-1, WCS-1, and WS-1 produce secondary fractures under the stress. The fractures of the WS-1 coal specimen exhibit the most intense shear and tensile deformation. The displacement dislocation of the localized deformation zones E, F, and G in the WCS-1 coal specimen increases at a stress of 0.28 MPa. The fracture formed at the WS end is a result of shear and tensile deformation. The CS end is affected by fractures at the WS end, which results in secondary fractures. However, The predominant mode of fractures is characterized by tensile deformation failure.

The CS-1 coal specimen exhibits the lowest fracturing degree, and localized deformation zones B, C, and D

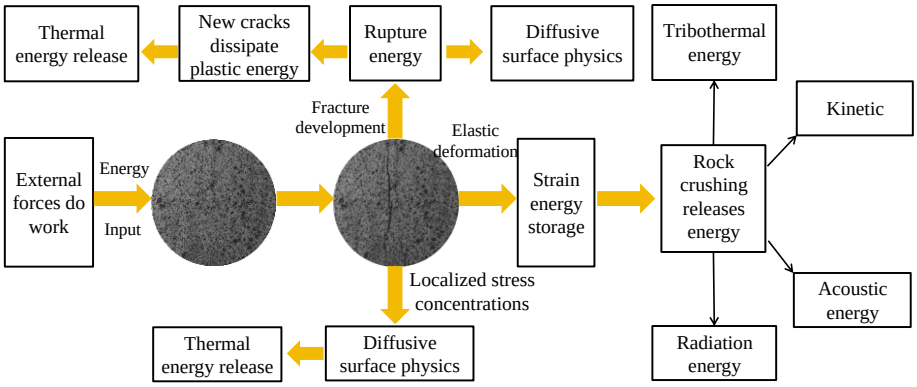

Fig 7 Energy transformation during the deformation and failure of coal specimens

increase at 1.08 MPa. The fracture form is mainly tensile deformation failure. The internal defects of coal specimens subjected to pressure-bearing water and CO_2 are more prone to fracturing and expanding, which leads to macroscopic fractures and subsequent failure.

3.3 Pre-peak energy evolution law of coal specimens

The deformation and damage evolution of coal rocks is accompanied by the accumulation, dissipation, and release of energy (Chen *et al*. 2017). The testing machine performs various loading tests on coal specimens subjected to the load. Mechanical energy is converted into the deformation energy of coal specimens. Part of energy is converted into elastic energy and stored in coal specimens. The other part is converted into dissipation when fractures occur inside coal specimens. Interpreting the stress-strain relationship of coal-rock specimens from an energy change perspective can enhance the understanding of the failure characteristics exhibited by these specimens (Fig. 7).

The Brazilian splitting test is an indirect method of measuring the tensile strength of coal specimens. It cannot obtain the deformation of coal specimens and calculate the pre-peak energy storage of coal specimens. The change in the internal energy of a thermodynamic system is equal to work done by heat transferred from the outside according to thermodynamic energy conservation law. Therefore, the failure mechanism of rocks can be revealed from an energy perspective.

The change law of U can elucidate the evolutionary character of pre-peak stored energy in coal specimens (Yagiz 2008, Zhang et al. 2020). Meanwhile, U can be regarded as mechanical energy exerted by the testing machine on coal specimens, namely.

$$U = \frac{1}{2} P_{max} S \tag{2}$$

Where P_{max} is the ultimate load of coal specimens, kN; S is the axial displacement corresponding to the ultimate load, mm.

Mechanical energy U of each group of coal specimens is calculated by Eq. (2) (Fig. 8). Coal specimens in the DC group exhibit the highest average mechanical energy U at 0.48 J, while the WS group demonstrates the lowest value at 0.15 J. The change law of U and uniaxial tensile strength is

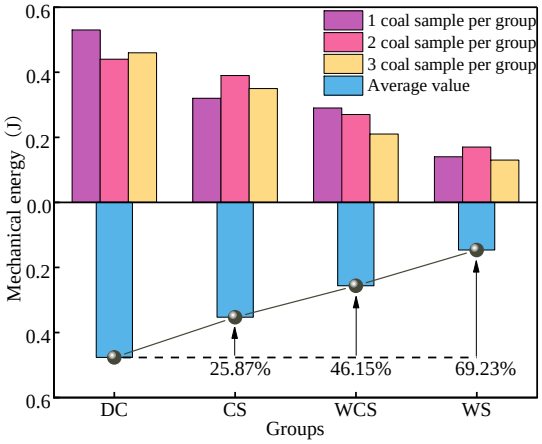

Fig. 8 Correlations between the mechanical energy of each group of coal specimens

consistent, indicating a gradual decreasing trend. Mechanical energy U of coal specimens in CS, WCS, and WS groups decreases by 25.87, 46.15, and 69.23% on average, respectively, compared with that in the DC group. The pre-peak energy storage of coal specimens changes with varying soaking conditions. The deformation and failure resistance of coal specimens are primarily influenced by the WS condition, followed by WS and CS conditions.

The conclusions are as follows. (1) The deterioration of the internal tensile mechanical property of coal specimens is primarily influenced by pressure-bearing water and CO_2. Then, increased initial damage inside specimens causes significant micro-fractures. Meanwhile, the difficulties in the relative slip of the original fracture surface are reduced, which damages the initial energy storage structure of specimens. (2) Stress concentration is likely to occur at coal rock defects under pressure-bearing water and CO_2 during the stress loading, which leads to the development and expansion of original fractures. Moreover, the original macroscopic tensile fracture surface is easier to slide, which causes secondary damage to the energy storage structure of coal specimens. Finally, ultimate damage occurs.

3.4 XRD/XRF test of coal specimens

X-ray diffusion (XRD) and X-ray fluorescence (XRF) were carried out to analyze factors influencing the variation

Table 2 Proportion of XRF test elements

Group	Na_2O (%)	MgO (%)	Al_2O_3 (%)	SiO_2 (%)	P_2O_5 (%)	SO_3 (%)	Cl (%)	$CaCO_3$ (%)	TiO_2 (%)	Fe_2O_3 (%)
DC	1.62	1.02	22.313	28.873	1.979	11.329	3.001	21.116	2.908	5.841
CS	1.952	1.235	15.562	20.395	2.347	13.295	3.023	29.875	3.107	3.392
WCS	2.224	2.495	10.554	20.674	1.287	13.244	4.758	34.328	2.112	8.324
WS	2.477	2.163	10.638	10.824	2.277	16.689	4.304	38.765	1.406	10.457

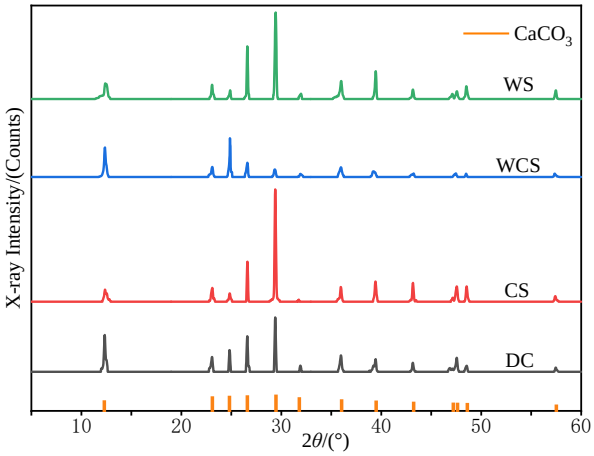

Fig. 9 XRD diffraction curve of $CaCO_3$ solid phases

in the tensile strength of coal specimens under different soaking conditions. The structural changes of coal specimen elements were determined by analyzing the crystal structure of coal specimens and the composition of material elements under different soaking conditions.

$CaCO_3$ solid phases exist in coal specimens under different soaking conditions (Fig. 9). The diffraction curve exhibits three apparent peaks, with the maximum reaching 33 and a corresponding diffraction angle of 29.47°. Coal specimens in the DC group exhibit a minimum $CaCO_3$ content, which accounts for 21.216% of the total. $CaCO_3$ in CS and WCS groups are 29.875 and 34.328%, respectively.

The WS group exhibits the most $CaCO_3$, accounting for 38.765% of the total (Table 2). $CaCO_3$ in coal specimens increases to varying degrees under different water-soaking conditions. $CaCO_3$ is produced the most under the WS condition, followed by the WCS condition. It is produced the least under the CS condition.

4. Deterioration mechanism of uniaxial tensile properties of coal specimens

The deterioration of pressure-bearing water and CO_2 on coal specimens primarily manifests in four aspects: (1) The original closed fracture surfaces in coal specimens are lubricated by water, which reduces its friction coefficient.

The difficulties in the relative slip of the fracture surface are reduced. (2) CO_2 exhibits strong extraction at a stress of 5 MPa. The functional structure of coal is altered by extracting the oxygen-containing functional groups (e.g., -C=-COOH). Therefore, the mechanical parameters of coal specimens decrease significantly in pressure-bearing water and CO_2. (3) CO_2 dissolves at the gas-liquid interface to form CO_3^{2-}, which drives Ca^{2+} to migrate. Therefore, Ca^{2+} migrates quickly to the gas-liquid interface and forms $CaCO_3$. The brittleness of $CaCO_3$, coupled with its low tensile strength, diminishes the internal cementing power of coal specimens and compromises their tensile strength. (4) Water and CO_2 naturally interact, which forms an acid solution (Gopinath and Mehra 2016, Yi *et al.* 2021), which dissolves soluble minerals in coal and forms microscopic structure defects. Originally non-connected micro-fractures spread out, which increases the pore area inside coal specimens. (5) Original micro-defects (e.g., fractures and pores) in coal specimens produce stress concentration under the stress. Besides, undischarged free water in specimens induces pore water pressure at micro-defects, which increases the tensile stress in the micro-defect stress concentration area. The occurrence and expansion of micro-fractures in the area form macroscopic fractures. Coal specimen failure occurs eventually. Fig. 10 shows the internal damage evolution of coal specimens under the DC condition and different soaking conditions.

SEM is used to analyze the microscopic characteristics of coal specimens' fractures to reveal deterioration inside coal specimens under different soaking conditions. The deterioration mechanism of coal specimens is revealed under pressure-bearing water and CO_2. Fig. 11 illustrates the SEM of fractures of DC-2, CS-2, WCS-2, and WS-2 after the Brazilian splitting test.

Fractures of the DC-2 coal specimen are obvious and intensified (Fig. 11). The DC-2 coal specimen exhibits few micro-fractures compared with the other three groups. Original fractures expand due to the stress. Micro-fractures of the CS-2 coal specimen increase significantly under the CO_2-soaking condition. The displacement of the fracture position is less pronounced compared to fractures observed in the DC-2 coal specimen due to increased fractures.

The WCS-2 coal specimen undergoes a chemical reaction under pressure-bearing water and CO_2. Dissolution occurs within a limited range in the coal specimen. Pores are mainly distributed in the region where the coal specimen is soaked in water. Significant dissolution occurs at the soaking site with low cementation. The WS-2 coal specimen dissolution is unevenly distributed with increased defect scale. Pores in the mineral particles are clear due to dissolution, which facilitates its expansion and the interconnection of fractures. The coal specimen transforms from an intensified to a loosely porous structure.

Software PCAS is used to identify and quantify its microscopic changes. Table 3 lists the parameters of calculated SEM images. Pores and fractures produced by

Table 3 Parameters of SEM recognized by PCAS

Group	Value taking	Average porosity (%)	Maximum area(μm²)	Average area(μm²)	Probability entropy
DC	Minimum-Maximum	4.47-7.32	6930-7430	124.33-131.76	0.8366-0.8391
	Mean value	5.87	7173.33	127.98	0.84
CS	Minimum-Maximum	6.73-8.56	8942-9478	135.63-140.24	0.8779-0.8825
	Mean value	7.65	9234	138.14	0.88
WCS	Minimum-Maximum	9.67-15.44	15356-15904	185.67-190.04	0.9343-0.9401
	Mean value	12.61	15629.33	188	0.94
WS	Minimum-Maximum	18.39-22.89	24178-25095	254.31-259.03	0.9665-0.9721
	Mean value	20.53	24631.67	256.61	0.97

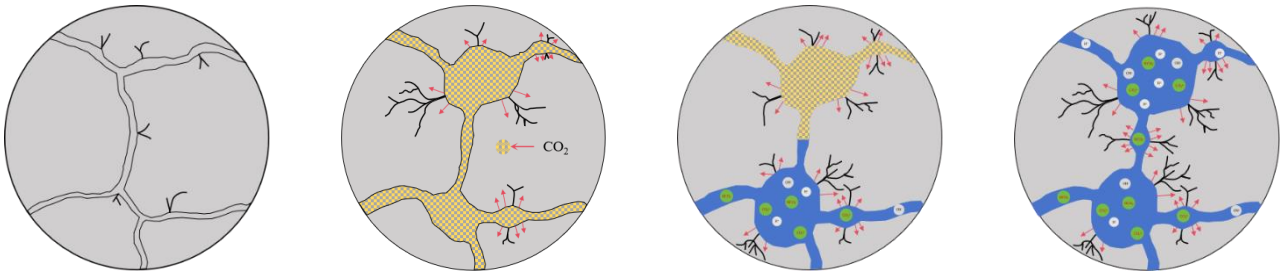

(a) DC (b) CS (c) WCS (d) WS

Fig. 10 Internal damage evolution of coal specimens

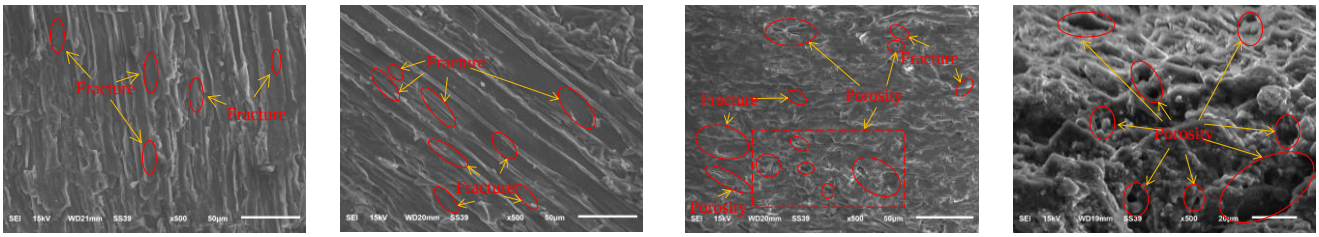

(a) DC-2 coal specimen (b) CS-2 coal specimen (c) WCS-2 coal specimen (d) WS-2coal specimen

Fig. 11 SEM of coal specimens' fractures

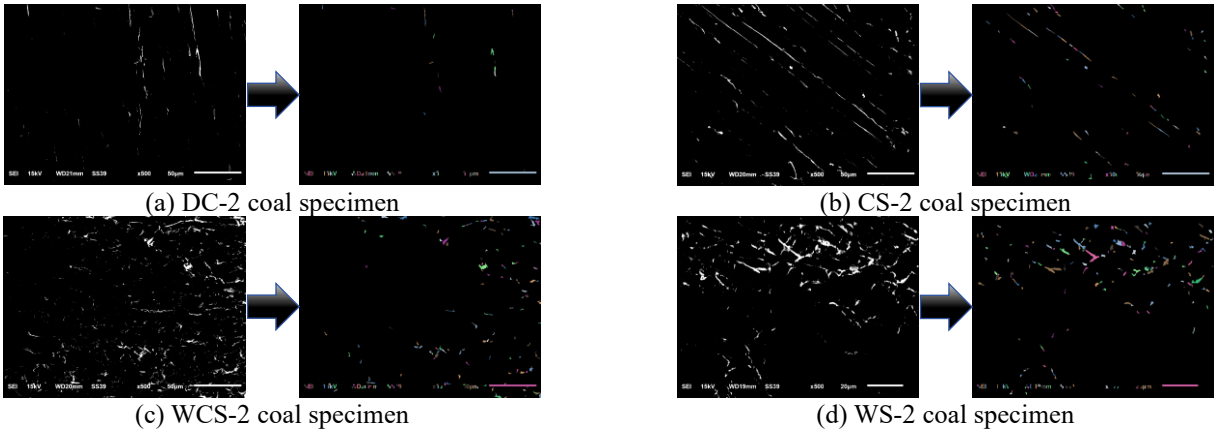

(a) DC-2 coal specimen (b) CS-2 coal specimen

(c) WCS-2 coal specimen (d) WS-2 coal specimen

Fig. 12 Binary images of the fracture surface of coal specimens

coal specimens are analyzed under different soaking conditions. Vector diagrams and rose diagrams of results are displayed through binarization in terms of pore recognition.

The black region is the non-porous area of the coal specimen, while the colored region represents the porous area. The fractures and pores of the WS-2 coal specimen (Fig. 12) exhibit a significantly greater magnitude and broader range compared to the other three groups.

Fig. 13 shows the relationship among the average porosity, maximum pore area, and probability entropy of the fracture surfaces of the same coal specimens under DC and soaking conditions. The average porosity of the DC group is the lowest (5.87%) (Fig. 13(a)). The average porosity of CS, WCS, and WS groups increases under varying soaking conditions, by 7.65, 12.61, and 20.53%, respectively. The porosity of the WS group increases the most, 249.55% of

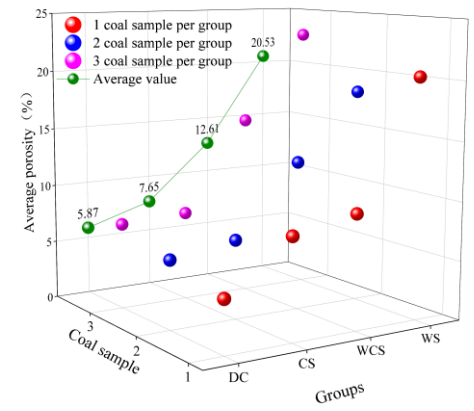

(a) Average porosity

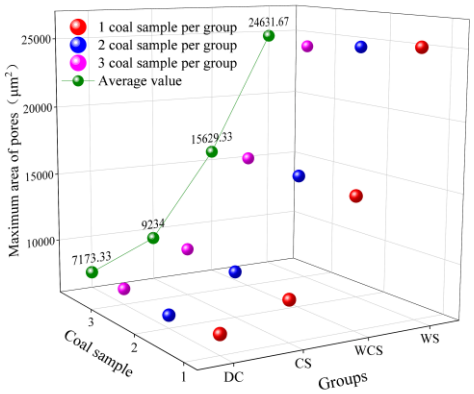

(b) Maximum area of pores

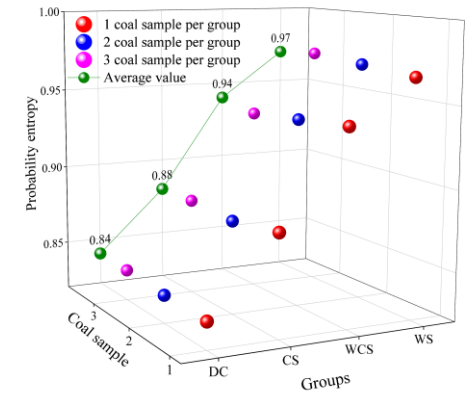

(c) Probability entropy

Fig 13 Relationship between the parameters of coal specimens' fracture surfaces and soaking conditions

the average porosity for the DC group. The increase in porosity of the CS and WCS groups is relatively small compared to that of the WS group. They are 0.19 and 114.76% of the average porosity of coal specimens in the DC group, respectively. The maximum pore areas of the four groups of coal specimens increase by 28.73, 117.88, and 243.38%, respectively, due to various soaking conditions (Fig. 13(b)).

The erosion and dissolution of coal specimens are intensified due to varying soaking conditions. Hydrolysis changes the pH of soaked water and coal specimens. Therefore, their mechanical properties are influenced. The acidic solution formed by pressure-bearing water and CO_2 penetrates between particles along the original fractures of coal specimens. The mineral components in coal specimens are dissolved in the acidic solution, which increases the number and area of pores. Micro-fractures rupture and expand rapidly, and macroscopic voids appear. Therefore, the average porosity and maximum porosity area of coal specimens increase.

The arrangement of microstructure units can be observed through probability entropy, which is an indicator to describe the directionality of pores. The probability entropy index of the directionality parameters of microscopic pores in SEM ranges from 0 to 1 determined through PCAS. Pores in the image exhibit consistent orientation when probability entropy is 0. Their directions are random (Gan 2019) when the index is 1. The pore entropy of coal specimens' fracture surfaces is calculated under various soaking conditions (Fig. 13(c)). The entropy of specimens in the CS, WCS, and WS groups increases by 5.08, 11.89, and 15.72%, respectively, compared with the DC group. Coal specimens show obvious fracturing effects when subjected to pressure soaking as well as pressure-bearing water and CO_2. The number and area of pores inside coal specimens increase, and the directivity deteriorates.

5. Conclusions

Uniaxial tensile strength tests were carried out on coal specimens under different soaking conditions. The influence of pressure-bearing water and CO_2 on the deterioration mechanism of coal rocks' tensile strength was revealed based on the failure intensity law under various soaking conditions. The conclusions are as follows.

(1) The stress-time curve of coal specimens underwent intensified fracture, unstable fracture development, and post-fracture stages. The tensile strength of coal specimens was reduced due to prolonged soaking. The WS condition affected greatest on the deterioration of coal specimens' tensile strength, followed by the WCS condition. The CS condition had the least effect.

(2) The fracture propagation of coal specimens showed different change law under various soaking conditions. Coal specimens formed a localized deformation zone at main fractures due to stress, which resulted in new fractures. Fracture propagation was more pronounced under the WCS condition compared to the CS condition. Besides, the displacement dislocation of the water-soaking end changed more frequently than that of the gas-soaking end. Therefore, the deterioration of coal specimens' tensile strength was more pronounced under the WS condition compared to the CS condition. Moreover, the deterioration of coal specimens' tensile strength was more significant when subjected to pressure-bearing water and CO_2 compared to exposure solely to CO_2.

(3) The elemental content of coal specimens changed under different soaking conditions. $CaCO_3$ increased when coal specimens were subjected to pressure-bearing water and CO_2. Coal specimens showed increased brittleness and a significant decrease in tensile strength.

(4) The deterioration of coal specimens' tensile properties was significantly affected by the water-soaking condition based on the results from different soaking conditions. The initial energy storage structure of coal specimens was damaged due to changes in soaking conditions. The pre-peak energy storage of specimens was reduced, so mechanical energy decreased in the test. Mineral particles inside specimens were eroded and dissolved by water and CO_2. The average porosity increased, and the internal structure of coal specimens transformed from intensified to porous. The defect scale increased, while the deformation and failure resistance decreased. Then, the deterioration of coal specimens' tensile properties increased.

Acknowledgements

This work was supported by National Natural Science Foundation of China(52374127); the Key supported project of the National Natural Science Foundation of China Regional Innovation and Development Joint Fund (U23A20600); Major Basic Research Project of Shandong Provincial Natural Science Foundation (ZR2024ZD22); Shandong Province Higher Educational Youth Innovation Science and Technology Support Program (2023KJ302).

References

Akin, I.D. and Likos, W.J. (2017), "Brazilian tensile strength testing of compacted clay", *Geotech. Test. J.*, **40**(4), 608-617. https://doi.org/10.1520/GTJ20160180.

Bai, Q.S., Tu, S.H. and Zhang, C. (2016), "DEM investigation of the fracture mechanism of rock disc containing hole(s) and its influence on tensile strength", *Theor. Appl. Fract. Mech.*, **86**, 197-216. https://doi.org/10.1016/j.tafmec.2016.07.005.

Bligen, C., Homberger, S. and Weiberg, K. (2019), "Phase-field fracture simulations of the Brazilian splitting test", *Int. J. Fract.*, **220**(1), 85-98. https://doi.org/10.1007/s10704-019-00401-w.

Chen, W., Liu, J, Peng, W.Q., Zhao, Y.L., Luo, S.L., Wan, W., Wu, Q.H., Wang, Y.Z., Li, S.N., Tang, X.Y., Zeng, X.T., Wu, X.F., Zhou, Y. and Xie, S.L. (2023), "Aging deterioration of mechanical properties on coal-rock combinations considering hydro-chemical corrosion", *Energy*., 282. https://doi.org/10.1016/j.energy.2023.128770.

Chen, X.M., Zhang, H.W., Wu, Y.P., Jiao, H.Z., Yang, L.H., Wang, Q.T. and Zhang, W.X. (2022), "Micro-mechanism of uniaxial compression damage of layered cemented backfill in underground mine", *Materials*, **15**(14), 4846. https://doi.org/10.3390/ma15144846.

Chen, Z.Q., He, C., Wu, D., Xu, G.W. and Yang, W.B. (2017), "Fracture evolution and energy mechanism of deep-buried carbonaceous slate", *Acta Geotech.*, **12**(6), 1-18. https://doi.org/10.1007/S11440-017-0606-5.

Gan, J.J. (2019), "Experimental study on the microstructure of the lacustrine soft clay after different consolidation deformations based on SEM", *IOP Conf. Ser.: Earth Environ. Sci.,* 304. https://doi.org/10.1088/1755-1315/304/5/052076.

Gong, S., Zhou, L., Wang, Z. and Wang, W. (2021), "Effect of bedding structure on the energy dissipation characteristics of dynamic tensile fracture for water-saturated coal", *Geofluids*. https://doi.org/10.1155/2021/5592672.

Gopinath, S. and Mehra, A. (2016), "Carbon sequestration during steel production: Modelling the dynamics of aqueous carbonation of steel slag", *Chem. Eng. Res. Des.*, **115**, 173-181. https://doi.org/10.1016/j.cherd.2016.09.010.

Guo, W.Y., Zhang, W., Zhang, C.G. and Chen, Y. (2024), "Experimental study on the deformation localisation and acoustic emission characteristics of coal in Brazilian splitting tests", *Scientific Reports*, 12. https://doi.org/10.1038/s41598-022-10332-7.

Guo, Y.X., Zhao, Y.H., Wang, S.W., Feng, G.R., Zhang, Y.J. and Ran, H.Y. (2021), "Stress-strain-acoustic responses in failure process of coal rock with different height to diameter ratios under uniaxial compression", *J. Cent. South Univ.*., **28**(6), 1724-1736. https://doi.org/10.1007/s11771-021-4729-3.

Heidari, M., Khanlari, G.R., Momeni, A.A. and Jafargholizadeh, H. (2011), "The relationship between geomechanical properties and weathering indices of granitic rocks, Hamedan, Iran", *Geomech. Geoeng*., **6**(1), 59-68. https://doi.org/10.1080/17486021003706580.

Hu, W.Y., Zhou, J.J. and Yan, L.Y. (2010), "Study on environment and safety disasters from abandoned coal mines", *J. Xi'an Univ. Sci. Technol.*, **30**(4), 436-440. https://doi.org/10.13800/j.cnki.xakjdxxb.2010.04.014.

Ji, L., Dong, J.H., Kienberger, T., Huang, J., Liu, F., Wang, W., Huang, Y.L. and Gao, H.D. (2023), "Quantitative assessment and development utilization modes of space resources in closed and abandoned mines", *Energy Sources, Part A*. https://api.semanticscholar.org/CorpusID:260860088.

Komurlu, E., Kesimal, A. and Demir, S. (2016). "Experimental and numerical analyses on determination of indirect (splitting) tensile strength of cemented paste backfill materials under different loading apparatus", *Geomech. Eng.*, **10**(6), 775-791. https://doi.org/10.12989/gae.2016.10.6.775.

Lbishi, G., Genis, M. and Yavuz. M. (2022), "Post-pillars design for safe exploitation at Trepca hard rock mine (Kosovo) based on numerical modeling", *Geomech. Eng.*, **5**(28), 463-475. https://doi.org/10.12989/gae.2022.28.5.463.

Li, W., Guan, J., Yan, Y. and Wang J. (2023), "Abandoned coal tunnel survey by multiscale window analysis of Rayleigh waves", *J. Appl. Geophys*., https://doi.org/10.1016/j.jappgeo.2023.105126.

Li, Y., Guan, J.B., Yan, Y.W. and Wang, J.Q. (2023), "Abandoned coal tunnel survey by multiscale window analysis of Rayleigh waves", *J. Appl. Geophys.*, **215**, 105126. https://doi.org/10.1016/j.jappgeo.2023.105126.

Li, Y.Y., Zhang, S.C., Yang, Y.M., Chen, H.R., Li, Z.K. and Ma, Q. (2022), "Study on the water bursting law and spatial distribution of fractures of mining overlying strata in weakly cemented strata in West China". *Geomech. Eng.*, **28**(6), 613-624. https://doi.org/10.12989/gae.2022.28.6.613.

Liu, S.Q., Wang, H.L., Xu, W.Y., Qu, X. and Xie, W.X. (2020), "Numerical Brazilian split test of pre-cracked granite with randomlydistributed micro-components", *Eng. Comput*., **37**(8), 2641-2657. https://doi.org/10.1108/EC-03-2019-0123.

Lyu, K., Jiang, N., Yin, D.W., Meng, S.Y., Gao, Z.Y. and Lyu, T. (2024), "Deterioration of compressive properties of coal rocks under water and gas coupling", *J. Cent. South Univ.*, **31**(2), 475-493. https://doi.org/10.1007/s11771-024-5583-x.

Miehe, C., Hofacker, M. and Welschinger, F. (2010), "A phase field model for rate-independent crack propagation: Robust algorithmic implementation based on operator splits", *Comput. Method. Appl. M.*, **199**(45-48), 2765-2778.

https://doi.org/10.1016/j.cma.2010.04.011.
Morris, A., Silver, D., Ferguson, D. and Thayer, S. (2005), "Towards topological exploration of abandoned mines", *ICRA*, 2117-2123. https://doi.org/10.1109/robot.2005.1570426.
Qu, J.L. and Tao, H. (2019), "Strength and deformation behavior of Shanghai andesite under various strain rates in uniaxial loading test", *Geomech. Geoeng*., **16**(1), 44-51. https://doi.org/10.1080/17486025.2019.1645364.
Shi, L.Q., Wang, Y., Qiu, M., Gao, W.F. and Zhai P.H. (2019), "Application of three-dimensional high-density resistivity method in roof water advanced detection during working stope mining", *Arabian J. Geosci.*, **12**, 464. https://doi.org/10.1007/s12517-019-4586-7.
Song, H., Zhao, Y., Wu, Y., Li, X.H., Gong, Z.X., Sun, Z., Jiang, Y.D. and Guo, Z.H. (2023), "Effect of water on the damage and energy dissipation feature of coal under uniaxial cyclic loading–unloading condition", *Energ. Sci. Eng.*, **11**, 4092-4107. https://doi.org/10.1002/ese3.1565.
Vásárhelyi, B. and Ván, P. (2006), "Influence of water content on the strength of rock", *Eng. Geol.*, **84**(1-2), 70-74. https://doi.org/10.1016/jenggeo.2005.11.011.
Wang, Y.Q., Wang, X., Zhang, J.S., Yang, B.S., Zhu, W.J. and Wang, Z.P. (2022), "Similar experimental study on retaining waterproof coal pillar in composite strata mining", *Sci. Rep.*, **12**, 1366. https://doi.org/10.1038/s41598-022-05369-7.
Xia, Z.H., Jiang, N. and Yang, H.S. (2020), "Effect of multiple hole distribution and shape based on particle flow on rocklike failure characteristics and mechanical behavior", *Adv. Civ. Eng.*, 2020. https://doi.org/10.1155/2020/8822225.
Xie, D., Du, Z., Han, C., Han, J., Wei, J. and Yan, J. (2023), "Prediction of the water inrush risk from an overlying separation layer in the thick overburden of a thick coal seam", *Sustainability*, **15**(18), 13988. https://doi.org/10.3390/su151813988.
Yagiz, S. (2008), "Assessment of brittleness using rock strength and density with punch penetration test", *Tunn. Undergr. Sp. Tech*., **24**(1), 66-74. https://doi.org/10.1016/j.tust.2008.04.002.
Yang, S.Q. and Huang, Y.H. (2015), "Particle flow study on strength and meso-mechanism of Braziliansplitting test for jointed rock mass", *Acta Mech. Sin.*, **30**(1), 189-201. https://doi.org/10.1007/s10409-014-0076-z.
Yi, Y.R., Lin, Y., Du, Y.C., Bai, S.Q., Ma, Z.L. and Chen, Y.G. (2021), "Accelerated carbonation of ladle furnace slag and characterization of its mineral phase", *Constr. Build. Mater.*, **276**, 122235. https://doi.org/10.1016/j.conbuildmat.2020.122235.
Yin, D.W., Ding, Y.S., Jiang, N., Li, F.X., Zhang, J.C. and Xu, H.H. (2022), "Mechanical properties and damage characteristics of coal samples under water immersion pressure", *Lithos*, **2022**(10), 1278783. https://doi.org/10.2113/2022/1278783.
Yin, H., Zhao, H., Xie, D., Sang, S.Z., Shi, Y.L. and Tian, M.H. (2019), "Mechanism of mine water inrush from overlying porous aquifer in Quaternary: a case study in Xinhe Coal Mine of Shandong Province", *Arab. J. Geosci.*, **12**(163). https://doi.org/10.1007/s12517-019-4325-0.
Zhang, C., Bai, Q. and Han, P. (2023), "A review of water rock interaction in underground coal mining: problems and analysis", *Bull. Eng. Geol. Environ.*, **82**, 157. https://doi.org/10.1007/s10064-023-03142-2.
Zhang, H., Lu, C.P. and Wang, H.Y. (2020), "Numerical investigation on crack development and energy evolution of stressed coal-rock combination", *Int. J. Rock Mech. Min. Sci.*, **133**, 104417. https://doi.org/10.1016/j.ijrmms.2020.104417.
Zhang, K., Zhang, Y.C., Zhang, S., Ren, J.X., Zhang, L., Zhang, R.J. and Cui, Y.Q. (2023), "Study on the energy evolution mechanism of coal and rock with impact tendency under different strain rates", *Sci. Rep*, **13**(1). https://doi.org/10.1038/s41598-023-41094-5.
Zhao, K., Gu, S.J., Yan, Y.J., Li, Q., Xiao, W.Q. and Liu, G.Q. (2018), "Rock mechanics characteristics test and optimization of high-efficiency mining in Dajishan tungsten mine", *Geofluids*, 1-11. https://doi.org/10.1155/2018/8036540.
Zhao, Y.X., Liu, S.M., Jiang, Y.D., Wang, K. and Huang, Y.Q. (2016), "Dynamic tensile strength of coal under dry and saturated conditions", *Rock Mech. Rock Eng.*, **49**, 1709-1720. https://doi.org/10.1007/s00603-015-0849-0.

GC